Catena 249 (2025) 108695

Contents lists available at ScienceDirect

Catena

journal homepage: www.elsevier.com/locate/catena

Divergent responses of soil aggregate-associated organic carbon fractions and carbon flow pathways to land-use changes in karst ecosystems: Insights from $\delta^{13}C$ signature

Xiai Zhu [a,b,*], Youxin Shen [a,b], Xia Yuan [a,b,c], Ashutosh Kumar Singh [a,b], Liya Jin [a,b,c], Bin Yang [a,b], Chuang Yuan [a,b], Xiaojin Jiang [a,b], Wenjie Liu [a,b,*]

[a] Key Laboratory of Tropical Forest Ecology, Xishuangbanna Tropical Botanical Garden, Chinese Academy of Sciences, Menglun 666303, PR China
[b] State Key Laboratory of Plant Diversity and Specialty Crops, Chinese Academy of Sciences, Beijing 100093, PR China
[c] College of Ecology and Environmental Science, Yunnan University, Kunming 650500, PR China

ARTICLE INFO

Dataset link: Karst soil carbon (Original data)

Keywords:
Soil aggregates
Labile OC
^{13}C natural abundance
C stabilization pathway
Karst ecosystems
Vegetation restoration

ABSTRACT

Land-use changes accompanying revegetation improve the sequestration of soil organic carbon (SOC) by accelerating aggregate formation. However, the intrinsic mechanisms of long-term C flow and sequestration following land-use changes in karst ecosystems remain largely unclear. We examined variations in aggregate-associated OC fraction and C flow pathways across four karst land uses (cropland, grassland, shrubland, and forestland). Result showed that agricultural cultivation disrupted soil aggregates and contributed to SOC depletion. Aggregate stability, labile and recalcitrant OC stocks generally increased along the vegetation restoration. The OC contents of bulk soils exhibited a strong positive correlation with the OC contents and mass proportions of macro- and micro-aggregates. Proportions of labile organic carbon (LOC) to SOC in the topsoil reduced with decreasing aggregate sizes, with being reshaped C pool by increasing LOC fraction in cropland. The $\delta^{13}C$ values of bulk soil decreased with the sequence of vegetation restoration, indicating a decreasing turnover rate and C loss as land cover shifts from grass to forest. The $\delta^{13}C$ was enriched as aggregate size decreased, with maximum value (−14.59 ‰) in the silt + clay fraction under grassland at the soil depth of 10–20 cm. Soil aggregate-associated C flow pathways predominantly occurred from macroaggregates to microaggregates and silt + clay size classes. This indicates that litter C input was incorporated into macroaggregates that were formed initially, while old SOC was often deposited in silt + clay fractions. Cropland demonstrated a greater intensity of C flows in topsoil compared to other land-use types, reflecting the fast turnover rate and loss of C under cropland soils. These results highlight that long-term soil labile and recalcitrant OC pools and C stabilization mechanisms at aggregate level are largely affected by land use. Appropriate land-use associated with grass and forest restoration maybe a promising way for enhancing SOC sequestration in karst areas.

1. Introduction

Soil organic carbon (SOC) formation and mineralization play critical roles in soil biogeochemical cycling and global climate regulation (Bossio et al., 2020; Peng et al., 2023; Zhao et al., 2024). Land-use changes driven by vegetation conversions typically alter organic matter input, microbial communities, and soil physiochemical properties, thereby influencing SOC stocks and ecosystem carbon cycling (Cheng et al., 2023; Dou et al., 2023). Numerous research indicate that natural-to human land transitions often deplete SOC and elevate carbon emissions (Gasser et al., 2020; Tian et al., 2021; Qin et al., 2024). Conversely, converting agricultural fields into ecosystems dominated by grasses, shrubs, and forests significantly contribute to the SOC stabilization and sequestration (Guo and Gifford, 2002; Deng et al., 2014; Pang et al., 2019; Yang et al., 2023). Understanding these dynamics is key to managing soil C and mitigating climate change.

Soil aggregates serve as structural components regulating organic carbon (OC) dynamics and nutrient cycling, with the distribution of

* Corresponding authors at: Key Laboratory of Tropical Forest Ecology, Xishuangbanna Tropical Botanical Garden, Chinese Academy of Sciences, Menglun 666303, PR China.
E-mail addresses: zhuxiai@xtbg.ac.cn (X. Zhu), lwj@xtbg.org.cn (W. Liu).

https://doi.org/10.1016/j.catena.2024.108695
Received 24 October 2024; Received in revised form 3 December 2024; Accepted 25 December 2024
Available online 28 December 2024

particle size and their stability being crucial for soil quality and ecological processes (Ma et al., 2022; Xiao et al., 2022). Land-use transitions often result in the destruction or reformation of soil aggregates, thus affecting the physical protection for OC and its fractions (Liu et al., 2018a; Yu et al., 2023). Labile OC (LOC) fractions, such as easily oxidized OC (EOC), respond swiftly to land-use conversion and act as sensitive indicators for subtle variations in the SOC pool (Blair et al., 1995; Dou et al., 2023). Conversely, recalcitrant OC (ROC) is a relatively stable fraction involving long-period C storage (Liu et al., 2017). Interactions among soil particles frequently lead to divergent distribution of various OC fractions within aggregates of different sizes. In general, soil LOC fractions are predominantly found in macroaggregates, whereas ROC is more concentrated in microaggregates (Burns et al., 2013; Ma et al., 2022). Given that variations in SOC fractions within aggregates can influence soil C sequestration and nutrient supply, distinguishing and assessing labile and recalcitrant pools at the aggregate level is essential to comprehensively understand how land use affects SOC dynamics.

Stable C isotope signatures provide a powerful means to investigate SOC dynamics and turnover in terrestrial ecosystems, particularly in understanding historical shifts in C_3 and C_4 vegetation composition (Han et al., 2020; Rong et al., 2020; Shi et al., 2023). The kinetics of ^{13}C fractionation results in an enrichment of $\delta^{13}C$ in the residual organic matters, with C stabilization occurring in a sequence from more labile to more stable C pools (Werth and Kuzyakov, 2010; Wang et al., 2022; Liao et al., 2024). By integrating soil physical fractionation techniques with natural ^{13}C isotope analysis, we can gain insights into the dynamics and strength of C stabilization pathways both within and among soil aggregates (Liu et al., 2018a; Wang et al., 2022). Previous studies have documented that the main C flows among aggregates follow a trend from macroaggregates (acting as a 'source') to microaggregates (serving as a 'product') across various land uses (Gunina and Kuzyakov, 2014; Atere et al., 2020; Wang et al., 2022; Shi et al., 2023). Consequently, the age and stability of SOC generally increase as the soil aggregate size decreases and the soil depth increases (Guillaume et al., 2015; Xiao et al., 2022). Moreover, the distributions of labile and non-labile OC fractions within aggregates may contribute to diverse soil ^{13}C natural abundance (Werth and Kuzyakov, 2010; Wang et al., 2022). Thus, understanding the differences in SOC composition among aggregates is crucial for interpreting the C stabilization pathway through the $\delta^{13}C$ approach. Nevertheless, only a few studies have directly linked alterations in aggregate-associated OC composition to ^{13}C fractionation in order to explore the underlying mechanisms of soil C sequestration. Addressing this gap is essential for enhancing our understanding of soil C cycling and its response to land-use changes.

Karst landforms cover 12–15 % of the Earth's land area, with the largest concentration in Southwestern China (Pang et al., 2019; Han et al., 2020). Prolonged deforestation for agricultural purposes has led to significant ecosystem degeneration characterized by water and soil loss, along with the emergence of karst rocky desertification in this area (Wang et al., 2019; Liu et al., 2020). Facing these environmental issues, several ecological rehabilitation projects have been implemented for returning abandoned croplands to grasslands, shrublands or forest since the early 21st century (Wang et al., 2023). Earlier research has explored how land-use changes involving vegetation restoration affected total SOC levels, aggregate distribution, and $\delta^{13}C$ composition within soil profiles in karst ecosystems (Liao et al., 2015; Han et al., 2020; Zheng et al., 2022). For example, Zhang et al. (2023) noted that EOC contents slightly increased with vegetation restoration in a tropical karst area, Southwest China. Liu et al. (2020) reported that the relationships between SOC concentrations and aggregate-associated $\delta^{13}C$ values showed that SOC stabilization was enhanced following agricultural abandonment in the karst region. However, the ecological fragile karst region of Southwest China has suffered severe soil erosion and nutrient loss. This often induces redistribution of organic matter in the soil profile, resulting in disordered records of natural ^{13}C-abundance (Liu et al., 2020). Moreover, variation of plant composition as vegetation restoration under land-use change can alter aggregate turnover and soil $\delta^{13}C$ composition (Liu et al., 2018b). Thus, the underlying mechanisms driving SOC (and its fractions) storage and the long-term C stabilization associated with soil aggregates amidst variations in land use still remain enigmatic (Liao et al., 2015; Liu et al., 2020).

In this study, space-for-time substitution and natural ^{13}C abundance approaches were applied to explore how land use (e.g., cropland, grassland, shrubland and forestland) impacts C transfer and sequestration in karst soils. The objectives were: a) analyzing SOC and its labile fraction distribution across land uses; b) assessing C isotope composition changes in bulk soil and different-sized aggregates; and c) providing mechanistic insights into aggregate-associated C stabilization pathways under land-use transformation.

2. Materials and method

2.1. Study site

The study was conducted in the Stone Forest World Geo-Park, Shilin County (24°31′–25°04′N, 103°11′–103°40′E), Yunnan Province, China (Fig. 1). The park is renowned for its distinctive karst landscapes, characterized by pinnacles, cones, and collapse depressions. Local climate is dominated by a subtropical monsoon type, which features an average temperature of 16.8 ℃ and an annual rainfall of 856 mm measured over the past decade (2014–2023). The majority of the rainfall, ranging from 76 % to 89 %, falls in the rainy season (from May to October). The primary soil type in the study site is Calcareous lithosols, classified as Haplic Acrisol according to the FAO-UNESCO system (FAO, 1998), with further soil properties detailed in Table 1.

The karst region originally boasted semi-evergreen broadleaved forests. The forestland mostly dominated by perennial evergreen plants, such as *Cyclobalanopsis glaucoides*, *Pistacia weinmannifolia*, *Olea yunnanensis*, and *Neolitsea homilantha*, often mixed with some deciduous species, such as *Pistacia chinensis*, *Carpinus mobeigiana*, and *Albizia mollis* (Zhao et al., 2020). However, in the 1960 s, extensive deforestation for agricultural purposes had led to a transformation of these original forests into neighboring croplands. Meanwhile, firewood and grazing activities by the local residents had degraded the original vegetation into patchy grasslands or shrublands. Thanks to ecological restoration projects led by the Chinese government, the degraded shrub and grass community has started to recover naturally in these karst regions (Yu et al., 2023). The current vegetation status for these land use types has been maintained and preserved for over 20 years (Zhao et al., 2020). Cropland in the region followed a summer maize (*Zea mays*) to winter wheat (*Triticum aestivum*) rotation. Conventional agricultural practices were adopted including plowing, chemical weeding, and annual compound fertilizer application at quantities of 180 ha^{-1}, 75 kg P ha^{-1}, and 60 kg K/ha during the maize planting season. No fertilizer was applied during the wheat planting season. The aboveground crop biomass was harvested and removed, whereas the crop stubble was left in the soil. The grasslands were composed of a few annual herbaceous species including *Heteropogon contortus*, *Oplismenus compositus*, and *Themeda triandra*, while the shrublands were characterized by *Spiraea salicifolia*, *Pyracantha fortuneana*, *Sophora viciifolia*, *Bidens pilosa*, and *Diospyros duetorum*.

2.2. Field sampling

Soil samples were meticulously collected from various land-use patterns, including cropland, grassland, shrubland, and forestland in April of 2023. To ensure accurate comparison, a total of 12 quadrats were established, with three 10 m × 10 m quadrats allocated to each land use. Each quadrat was strategically placed with a distance of < 50 m between them, ensuring consistent factors such as elevation, soil type, slope gradient, and land-use history. The methodical approach involved

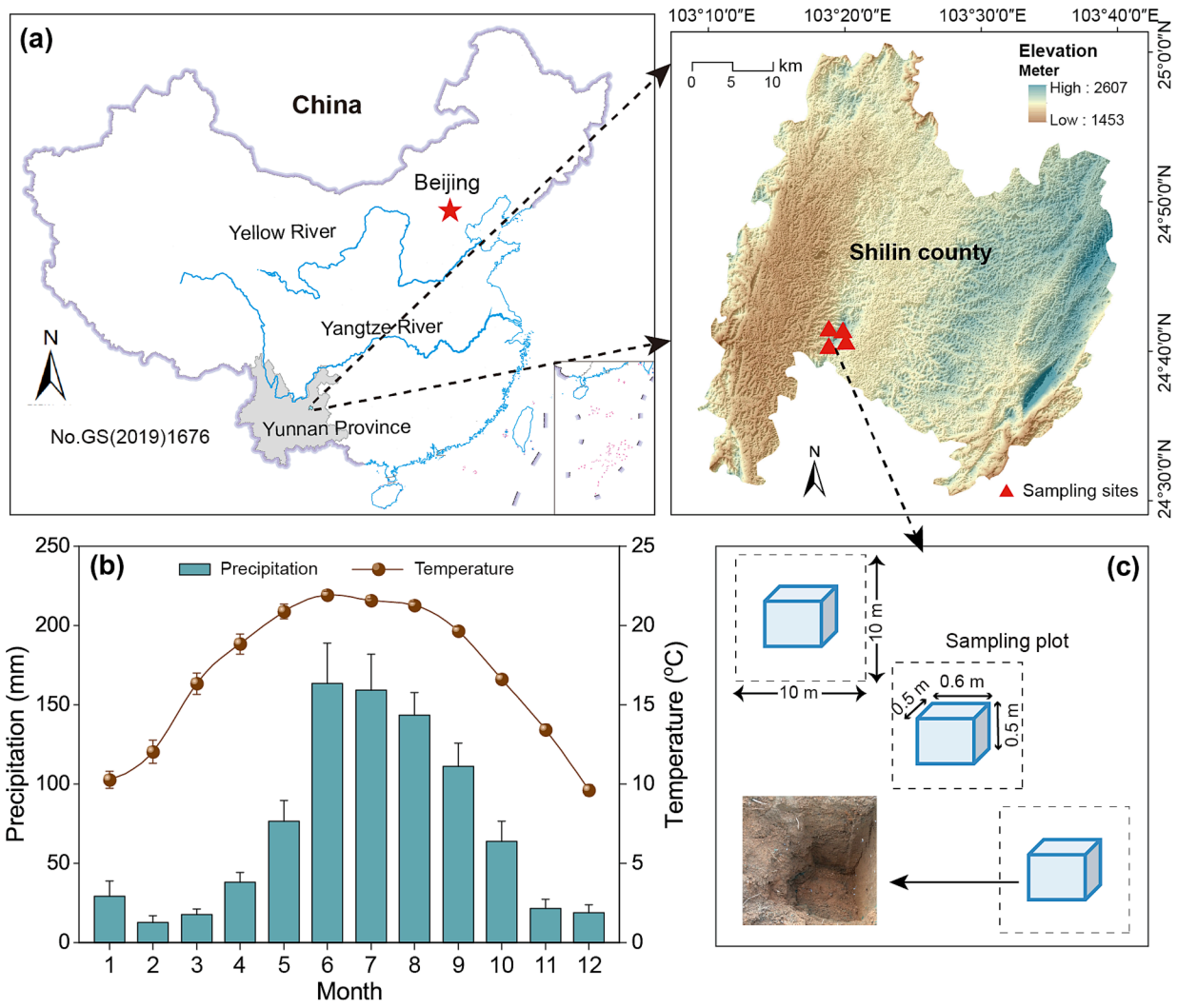

Fig. 1. Map showing the geographical location (a), mean monthly precipitation and temperature (b) during 2014–2023, and diagram of sampling design for soil collection (c) in the study area.

removing the litter layer before extracting soil samples. A vertical pit of specific dimensions (60 cm long × 50 cm wide × 50 cm deep) was dug at the center of each quadrat. Stainless-steel cutting rings (200 cm^3) were inserted horizontally to collect intact soil cores from 0 to 5, 5–10, 10–20 and 20–40 cm depths. Here, soil samples were collected at dense depths due to the sensitive responses of SOC fractions and stabilization processes in the surface soil to land use changes. In total 96 soil cores (4 land-use patterns × 4 depths × 6 replications) were collected to measure bulk density and soil porosity, following a standardized method as described by Pansu and Gautheyrou (2007). Additionally, composite samples were created by mixing soil from six random locations within the same depth in each quadrat. Upon removal of visible gravel and organic debris, the soil samples were transported to the laboratory for additional testing and analysis.

2.3. Soil aggregate fractionations

The study analyzed the distribution and stability of soil aggregates through a wet sieving procedure developed by Cambardella and Elliott. (1993). Firstly, 50 g of air-dried soil samples were carefully weighed on the basis of mass proportion of the different dry-sieved aggregate size classes. The soil samples were then transferred to the upper sieve of a series of six sieves that have different mesh sizes (5, 2, 1, 0.5, 0.25 and 0.053 mm). Subsequently, the soil samples were submerged in deionized water for 10 min and subject to vertical shaking at the 4-cm amplitude for 30 min. The aggregate samples retained on each sieve were meticulously gathered after shaking, dried in an oven at 60 ℃, and subsequently categorized and combined into four size classes: large (>2 mm) and small (2–0.25 mm) macroaggregates (LM and SM), microaggregates (0.25–0.053 mm, MI), and silt + clay classes (<0.053 mm, SC). Finally, the percentage of each size class of water-stable aggregate relative to the overall dry weight of the sample was calculated.

Soil structural stability were evaluated by examining factors including the mass proportion of water-stable aggregate > 0.25 mm (WSA, %), mean weight diameter (MWD, mm), and geometric mean diameter (GMD, mm) as computed below (Cheng et al., 2023):

$$\mathrm{WSA} = \frac{W_{0.25}}{W_t} \times 100 \quad (1)$$

$$\mathrm{MWD} = \sum_{i=1}^{n} X_i Y_i \quad (2)$$

$$\mathrm{GMD} = \exp\left[\frac{\sum_{i=1}^{n} W_i \ln X_i}{\sum_{i=1}^{n} W_i}\right] \quad (3)$$

where $W_{0.25}$ and W_t was weight (g) of aggregates larger than 0.25 mm and total weight of all aggregates, respectively; X_i indicated the average diameter (mm) of the i^{th} size class of aggregates, Y_i denoted the mass

Table 1
Soil basic physiochemical properties (0–40 cm) of each land use at the study site in the karst region, Southwest China.

Land-use type	Cropland	Grassland	Shrubland	Forestland
Soil moisture (%)	19.27 ± 0.35c	23.20 ± 0.94b	22.54 ± 0.93b	27.28 ± 1.32a
Bulk density (g cm^{-3})	1.11 ± 0.05a	1.13 ± 0.03a	1.07 ± 0.04a	1.09 ± 0.05a
Soil porosity (%)	53.77 ± 1.09b	58.78 ± 0.82a	54.32 ± 1.36b	53.93 ± 0.98b
Soil pH	6.74 ± 0.07b	7.15 ± 0.06a	5.95 ± 0.08c	5.76 ± 0.11c
Total nitrogen (g kg^{-1})	1.17 ± 0.08d	5.09 ± 0.15b	4.15 ± 0.14c	5.96 ± 0.43a
C/N	15.30 ± 0.65a	4.66 ± 0.34b	3.86 ± 0.44b	1.90 ± 0.55b
Total phosphorus (g kg^{-1})	0.78 ± 0.08a	0.83 ± 0.11a	0.73 ± 0.07a	0.67 ± 0.05a
Sand content (%)	14.92 ± 1.11a	15.92 ± 2.43a	19.00 ± 2.15a	15.00 ± 1.45a
Silt content (%)	37.17 ± 1.74a	34.58 ± 1.63ab	33.00 ± 2.85ab	30.42 ± 2.91b
Clay content (%)	47.92 ± 1.41b	49.50 ± 1.76ab	48.00 ± 1.74b	54.58 ± 3.13a

Note: Data are expressed as mean ± standard errors. Values with different lowercase letters indicate significant difference ($p < 0.05$) between different land uses.

proportion (%) of the i^{th} aggregate size class in relation to total sieved soil, and W_i signified the weight (g) of the i^{th} aggregate size class.

Soil stability index (St, %) was determined with a formula by Reynolds et al. (2009) to assess the soil's structural integrity:

$$St = \frac{1.724 \times SOC}{silt + clay} \times 100 \quad (4)$$

where 1.724 was the conversion factor from SOC to soil organic matter.

The calculation of SOC stocks in bulk soil (S_{BS}, Mg ha^{-1}), soil aggregates (S_{Ai}, Mg ha^{-1}), and contribution rate (S_{Ac}, %) of the aggregate size fraction to SOC content for each layer were conducted using the following equations (Rong et al., 2020; Shi et al., 2023; Cheng et al., 2023):

$$S_{BS} = \frac{H \times BD \times C}{10} \quad (5)$$

$$S_{Ai} = \frac{H \times BD \times Y_i \times C_i}{10} \quad (6)$$

$$S_{Ac} = \frac{Y_i \times C_i}{\sum_{i=1}^{n} Y_i \times C_i} \quad (7)$$

where H was the thickness (cm) of sampled soil depth, BD denoted bulk density (g cm^{-3}), C and C_i corresponded OC contents (g kg^{-1}) in various soil layers and in the i^{th} aggregate fraction, respectively. Y_i indicated mass proportion (%) of the i^{th} size of aggregate.

2.4. Soil properties and isotope analyses

The pH of the soil was tested using a digital pH meter. Soil texture was assessed with a laser particle size analyzer (Mastersiaer 3000, Malvern, UK). Soil total nitrogen was determined using the Kjeldahl acid-digestion method with an Auto-analyzer 3 (SEAL Analytical GmbH., Norderstedt, Germany). Total phosphorus was determined by molybdenum antimony spectrophotometry after wet digestion with $HClO_4$-HF. LOC content (represented by EOC here) was determined by UV- spectrophotometer after the oxidization with 333 mmol L^{-1} $KMnO_4$ (Blair et al., 1995; Liao et al., 2015). ROC content was determined by calculating the differences between TOC and LOC levels. The bulk soil and aggregate samples were treated with 1 M HCl for 24 h in order to eliminate the impact of carbonates on isotope measurement (Rong et al., 2020). Approximately 4 mg ground samples (passing through a 100-mesh sieve) were wrapped in tin capsules for the determination of TOC contents, as well as natural abundances of ^{13}C, using a MAT-253 Isotope Ratio Mass Spectrometer (Thermo Fisher) with a FLASH 2000 HT elemental analyzer (Thermo Fisher, USA). The $^{13}C/^{12}C$ ratio (where called R) in a sample was reported in relationship to the international standard (Vienna Pee Dee Belemnite, V-PDB; Li et al., 2020).

$$\delta^{13}C = \left[\frac{R_{sample}}{R_{standard}} - 1\right] \times 1000 \quad (8)$$

2.5. Soil OC sequestration and flow pathway

Gunina and Kuzyakov (2014) proposed a novel approach to elucidate the pathways of C transfer between different aggregate-sized classes. This method is based on the biological rule that ^{12}C turns over faster than ^{13}C chemically, often contributing to an accumulation of ^{13}C in older soil C (Liao et al., 2024). By calculating the variations in C isotopic composition ($\Delta^{13}C$) between $\delta^{13}C$ values of aggregates and $\delta^{13}C$ of bulk soil, it was possible to determine C flows among aggregate fractions and whether there was enrichment or depletion of ^{13}C within the aggregates (Shi et al., 2023). This method allowed for the identification of sources and products of C flows between aggregates (Wang et al., 2022). By arranging the different aggregate sizes into a systematic framework and using arrows to indicate connections between them, the movement of C ("source" to "products") could be visualized. The differences in $\Delta^{13}C$ values between aggregate fractions provided insights into the direction and relative probability of C flow. Specifically, a smaller difference accompanied by a wider arrow illustrated a higher probability of C transfer between the two aggregate size classes (Li et al., 2020).

2.6. Statistical analyses

All the data were assessed for homogeneity and normality using the Levene's and Shapiro-Wilk test, respectively. A log or square-root transformation was conducted if the conditions were not met. One- and two-way Analysis of Variance (ANOVA) along with the LSD statistic at a significance level of $p < 0.05$ were performed to estimate the impacts of land use, soil depth and their interactions on the aggregate distribution, stability indices, OC content and stock, and $\delta^{13}C$ values both in whole soil and aggregates. Pearson's correlation was used to assess correlations between various soil properties and aggregate-associated parameters. Additionally, general linear regression was employed to examine the relationship between soil depth, particle sizes and isotopic composition of aggregates. IBM SPSS Statistics 25 (IBM Corp., Armonk, NY, USA) and OriginPro 2024 (OriginLab Corp., Northampton, MA, USA) software were used in all statistical analyses.

3. Results

3.1. Fractions and stocks of SOC across various land uses

Land-use type and soil depth exerted significant impacts on SOC contents and stocks ($p < 0.01$; Fig. 2a–c). Forestland had the highest SOC stock in topsoil soil (0–10 cm; 41.34 Mg ha^{-1}), followed by grassland (30.16 Mg ha^{-1}), shrubland (21.40 Mg ha^{-1}), and cropland (19.16 Mg ha^{-1}). Across the entire soil profile (0–40 cm), the shrubland (61.52 Mg ha^{-1}) and cropland (75.72 Mg ha^{-1}) had lower SOC stocks than other types of land use.

No significant differences in the LOC stocks within the 0–10 cm depth were observed among land uses (Fig. 2e–f). However, the LOC stocks in 0–40 cm soil profiles exhibited significant differences ($p < 0.05$) between land uses, ranked as follows: cropland (45.15 Mg ha^{-1}) > grassland (44.98 Mg ha^{-1}) > forestland (42.63 Mg ha^{-1}) > shrubland (26.33 Mg ha^{-1}). Overall, the ROC stocks demonstrated similar

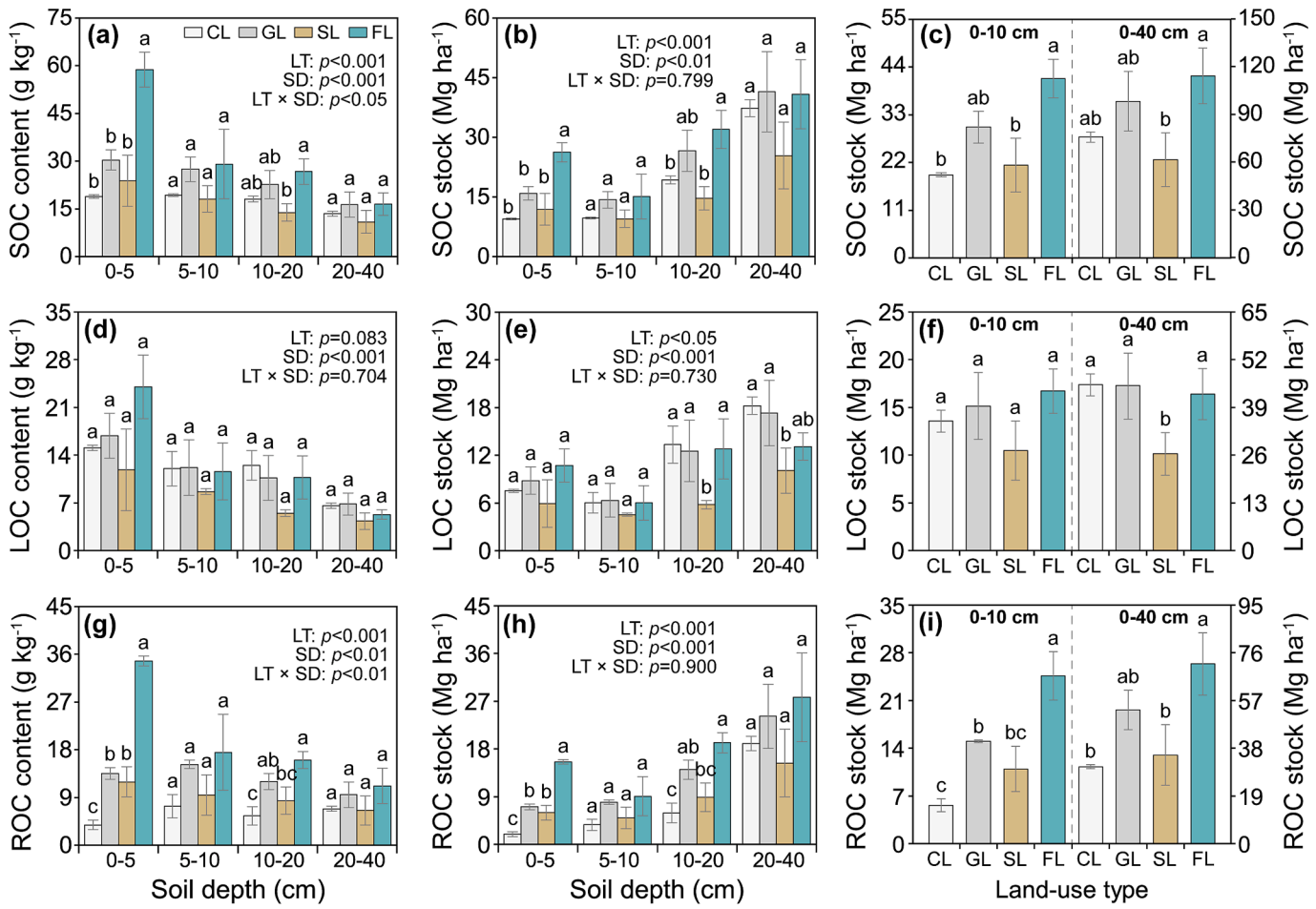

Fig. 2. Soil organic carbon (SOC), labile organic carbon (LOC) and recalcitrant organic carbon (ROC) contents and stocks along the soil profile, in the 0–10 cm (c) and 0–40 cm (d) soil layer under four land uses. Data are expressed as means and standard errors. Different lowercase letters within the same depth indicate significant differences ($p < 0.05$) among the land uses. LT × SD indicates the interaction effect of both land-use type (LT) and soil depth (SD). CL: cropland, GL: grassland, SL: shrubland, FL: forestland.

Table 2
Mass proportions of the soil aggregate size classes (%) under different land-use types.

Soil depth (cm)	Land-use type	Mass proportion of aggregate classes (%)			
		> 2 mm	2–0.25 mm	0.25–0.053 mm	< 0.053 mm
0–5	Cropland	30.76 ± 1.46dBC	53.58 ± 0.98aA	8.31 ± 0.41aB	7.36 ± 0.56aAB
	Grassland	61.06 ± 1.63bB	31.64 ± 1.23cA	2.64 ± 0.19bcA	4.68 ± 0.48bA
	Shrubland	49.07 ± 2.40cA	43.15 ± 2.29bA	3.55 ± 0.27bA	4.23 ± 0.26bA
	Forestland	69.56 ± 0.88aAB	23.80 ± 1.09 dB	1.85 ± 0.09cB	4.79 ± 0.48bA
5–10	Cropland	28.88 ± 1.03cC	51.80 ± 0.77aAB	10.11 ± 0.37aA	9.20 ± 0.75aA
	Grassland	71.66 ± 1.48aA	22.83 ± 1.47cB	1.93 ± 0.08cB	3.58 ± 0.12bB
	Shrubland	50.05 ± 5.01bA	40.95 ± 4.21bA	4.56 ± 0.56bA	4.44 ± 0.34bA
	Forestland	72.94 ± 1.18aA	21.91 ± 1.14cB	2.05 ± 0.09cB	3.09 ± 0.17bB
10–20	Cropland	36.45 ± 1.82bAB	48.79 ± 1.24aB	6.99 ± 0.37aC	7.77 ± 1.04aAB
	Grassland	68.72 ± 1.64aA	25.50 ± 1.58bAB	2.14 ± 0.07cB	3.63 ± 0.18bB
	Shrubland	44.75 ± 5.14bA	47.03 ± 4.73aA	4.51 ± 0.33bA	3.72 ± 0.30bA
	Forestland	59.76 ± 4.12aB	33.75 ± 3.95bB	2.30 ± 0.21cB	4.20 ± 0.22bAB
20–40	Cropland	38.89 ± 2.07bA	51.13 ± 1.87aAB	4.82 ± 0.23aD	5.17 ± 0.25aB
	Grassland	69.47 ± 2.77aA	25.38 ± 2.71bAB	1.70 ± 0.10cB	3.45 ± 0.11bB
	Shrubland	42.01 ± 5.04bA	50.29 ± 4.49aA	3.60 ± 0.44bA	4.10 ± 0.40abA
	Forestland	41.38 ± 5.36bC	51.05 ± 5.00aA	3.11 ± 0.22bA	4.46 ± 0.39abA
Summary of ANOVA (p values)					
Land-use type (LT)		<0.001	<0.001	<0.001	<0.05
Soil depth (SD)		<0.01	<0.001	<0.001	<0.001
LT × SD		<0.001	<0.001	<0.001	<0.001

Note: Data are expressed as mean ± standard errors. Values with different lowercase letters within the same soil depth (SD) indicate significant difference ($p < 0.05$) among land-use types (LT). Values with different uppercase letters under the same LT indicate significant difference ($p < 0.05$) between different SD. LT × SD indicates the interaction effect of both LT and SD.

variation patterns across land uses in each soil layer, except for the 20–40 cm layer (Fig. 2h–i). Within the 0–40 cm depth, the ROC stocks significantly differed from land-use types, with the decreasing order of forestland > grassland > shrubland > cropland.

3.2. Soil aggregate-size distribution and structure stability

Water-stable macroaggregates, specifically LM and SM (80.68 % to 94.86 %), dominated the composition of soil across different land uses and soil depths (Table 2). In contrast, microaggregates and silt + clay fractions made up a smaller proportion of the soil, ranging from 1.70 to 10.11 % and 3.09 to 9.20 %, respectively. Cropland soils had significantly lower WSA contents compared to other land uses, while the silt + clay fraction exhibited the opposite trend (Tables 2–3).

Aggregate stability was notably affected by land-use type and soil depth, as well as their interactions ($p < 0.05$; Table 3). Compared to cropland, the MWD of grassland, shrubland and forestland increased by 68.05 %, 27.88 % and 57.06 %, respectively; and the GMD increased by 125.17 %, 62.21 % and 111.99 %, respectively. The highest MWD and GMD values were observed in the 5–10 cm soil layer and the lowest in the 20–40 cm soil layer, excluding farmland. Overall, the St decreased with increasing soil depths, with grassland and forestland showing 1.21–2.92 times higher St than that under cropland.

The analysis of correlation between soil physicochemical properties and aggregate stability revealed that a positive relationship between BD and WSA, MWD and GWD in both cropland and shrubland (Fig. 3). Conversely, SP displayed negative correlations with WSA, MWD and GMD across all land-use types. Additionally, WSA, MWD and GMD were significantly correlated with silt content in shrubland and clay content in forestland ($p < 0.05$). Excluding cropland, St was found to have a significant positive relationship with SOC, LOC, ROC, TN and C/N in other land uses ($p < 0.001$).

3.3. The OC characteristics in soil aggregates

The distribution and amounts of OC within aggregates were found to be greatly affected by soil layers and land-use practices ($p < 0.05$; Fig. 4). OC contents within aggregates decreased with increasing soil depth under all land uses. In the topsoil layer (0–5 cm), OC contents in aggregates from grassland, shrubland and forestland were 41.09–76.61 %, 2.96–35.78 % and 127.69–265.48 % higher than that in cropland, respectively. Compared with cropland, the average OC stocks associated with LM fraction in other land-use types increased by 29.99 % to 203.32 % (Fig. 4b). The contribution of aggregates to SOC varied depending on particle size and land use ($p < 0.05$; Fig. 4c). For the 0–20 cm depth, macroaggregates contributed the most to SOC, accounting for 82.16–93.92 % across all land uses.

When OC of soil aggregates was separated into LOC and ROC, it was found that ROC was the dominant fraction in all aggregate-size classes, accounting for 37.92–89.55 % (Fig. 5). In the 0–5 cm topsoil, the highest LOC contents were observed in MI under forestland and in macroaggregates under cropland and grassland. Both LOC and ROC content decreased with soil depth in forestland. In the same soil depth, the ROC content in forestland aggregates was significantly higher (40.67–61.98 g kg^{-1}) compared to other land uses (11.09–27.29 g kg^{-1}), with the SC fraction having the highest ROC content. The proportion of LOC decreased as particle size decreased in the 0–5 cm soil aggregates, with cropland showing higher LOC proportions (28.57–62.08 %) than other land-use types (10.45–35.68 %).

3.4. Changes in $\delta^{13}C$ values of both bulk soil and its aggregates

Generally, the $\delta^{13}C$ values of the bulk soil exhibited a decrease pattern with vegetation restoration and an increase pattern with soil depth (Fig. 6). The highest $\delta^{13}C$ recorded in bulk soil was − 14.53 ‰ under grassland (10–20 cm), while the lowest value was − 26.23 ‰ under forestland (0–5 cm). As particle size decreased and soil depth increased, the $\delta^{13}C$ values within aggregates tended to rise across various land uses. This trend was evident in grassland where the maximum $\delta^{13}C$ (−14.59 ‰) was found in the silt + clay fraction, whereas the forestland's macroaggregates displayed the minimum $\delta^{13}C$ (−26.55 ‰). In addition, the difference ($\Delta^{13}C$) between $\delta^{13}C$ of aggregates and bulk soil demonstrated an upward trajectory with decreasing aggregate size (Fig. 6i–l), with the largest and smallest $\Delta^{13}C$ values occurring in the SC and LM fractions, respectively, under shrubland.

3.5. Pathways of C flow between soil aggregate fractions

The flow charts in Fig. 7 depicted the primary C flow pathways between different aggregate size classes across various land uses and soil

Table 3
Distribution of water-stable aggregate (> 2.5 mm; WSA), mean weight diameters (MWD), geometric mean diameter (GMD), and soil structural stability index (St) under four land uses.

Soil depth (cm)	Land-use type	WSA	MWD	GMD	St
0–5	Cropland	84.33 ± 0.80bB	2.46 ± 0.08 dB	1.24 ± 0.06dBC	4.01 ± 0.12bA
	Grassland	92.68 ± 0.55aB	4.02 ± 0.08bB	2.54 ± 0.10bB	5.51 ± 0.43bA
	Shrubland	92.21 ± 0.37aA	3.44 ± 0.12cA	2.08 ± 0.09cA	4.81 ± 1.17bA
	Forestland	93.36 ± 0.45aB	4.45 ± 0.04aAB	2.91 ± 0.05aAB	11.70 ± 0.80aA
5–10	Cropland	80.68 ± 0.93cC	2.33 ± 0.06cB	1.08 ± 0.05cC	3.90 ± 0.11aA
	Grassland	94.49 ± 0.15aA	4.56 ± 0.07aA	3.16 ± 0.08aA	5.59 ± 0.63aA
	Shrubland	91.00 ± 0.85bA	3.47 ± 0.25bA	2.25 ± 0.20bA	3.69 ± 0.69aA
	Forestland	94.86 ± 0.19aA	4.63 ± 0.06aA	3.28 ± 0.07aA	5.83 ± 2.14aB
10–20	Cropland	85.24 ± 1.28cB	2.75 ± 0.10bA	1.41 ± 0.08cB	3.57 ± 0.19bA
	Grassland	94.22 ± 0.20aA	4.41 ± 0.08aA	3.00 ± 0.09aA	4.67 ± 0.69abA
	Shrubland	91.77 ± 0.57bA	3.22 ± 0.26bA	2.09 ± 0.18bA	2.97 ± 0.45bA
	Forestland	93.50 ± 0.23abB	3.97 ± 0.20aB	2.65 ± 0.18aB	5.60 ± 0.68aB
20–40	Cropland	90.01 ± 0.33cA	2.92 ± 0.10bA	1.64 ± 0.07bA	2.72 ± 0.23aB
	Grassland	94.85 ± 0.12aA	4.46 ± 0.14aA	3.13 ± 0.13aA	3.74 ± 0.91aA
	Shrubland	92.30 ± 0.75bA	3.09 ± 0.25bA	2.04 ± 0.20bA	2.34 ± 0.73aA
	Forestland	92.43 ± 0.56bB	3.06 ± 0.27bC	2.00 ± 0.19bC	3.28 ± 0.66aB
Summary of ANOVA (p values)					
Land-use type (LT)		<0.001	<0.001	<0.001	<0.001
Soil depth (SD)		<0.001	<0.05	<0.05	<0.001
LT × SD		<0.001	<0.001	<0.001	<0.01

Note: Data are expressed as means and standard errors. Different lowercase letters within the same soil depth (SD) indicate significant differences ($p < 0.05$) among land-use types (LT). Different uppercase letters within the same LT indicate significant differences ($p < 0.05$) between SD. LT × SD indicates the interaction effect of both LT and SD.

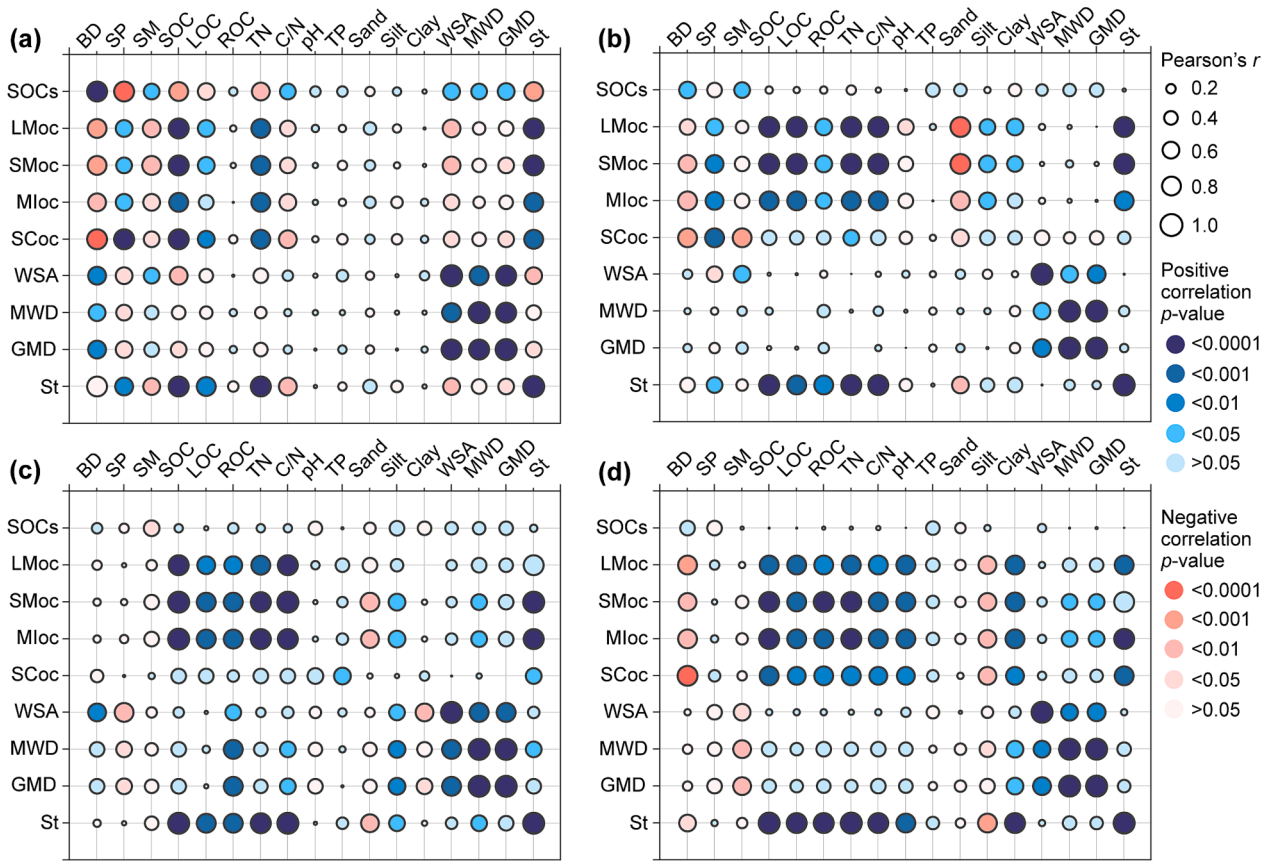

Fig. 3. Correlations between aggregate-associated parameters and soil physiochemical properties under cropland (a), grassland (b), shrubland (c) and forestland (d). BD: bulk density, SP: soil porosity, SM: soil moisture, SOC: soil organic carbon, LOC: liable organic carbon, ROC: recalcitrant organic carbon, TN: total nitrogen, C/N: carbon and nitrogen ratio, TP: total phosphorus, WSA: water-stable aggregate index, MWD: mean weight diameter, GMD: geometric mean diameter, St: soil structural stability index, SOCs: soil organic carbon stock, LMoc, SMoc, MIoc, and SCoc denote the organic carbon contents of large macroaggregates, small macroaggregates, microaggregates and silt–clay fraction, respectively.

depths. Generally, the majority of C flows (approximately 89 %) transferred from larger aggregates to smaller ones, with a few exceptions highlighted by red arrows. The C was observed to transition from macroaggregates (referred to as the "source") to the SC fraction (termed the "product") either directly or through the MI across all land-use types. The width of arrows illustrated that the intensity of C flows (or interactions) between aggregates, with cropland and forestland exhibiting greater magnitudes compared to grassland and shrubland. Furthermore, the most significant C flow typically occurred between large and small macroaggregates (LM and SM) or between microaggregates and silt + clay fraction.

4. Discussion

4.1. Variations in aggregate distribution and stability across different land uses

Significant changes in the distribution and stability soil aggregate were detected following land-use conversion in the current study (Tables 2–3). Specifically, the restoration of land use led to a substantial increase (2.54–17.57 %) in macroaggregate (> 0.25 mm) content, indicating that vegetation restoration effectively enhanced the soil aggregation which is crucial for soil structure and health. This result aligns with the finding of Yu et al. (2023) in a karst area in SW China, where afforestation also resulted in a significant increase in macroaggregates. On the other hand, cropland had higher levels of microaggregate and silt + clay compared to other land uses. This discrepancy was largely attributed to the impacts of frequent tillage and raindrop splash, which caused the breakdown of macroaggregates and the production of fine soil particles (An et al., 2021; Zhong et al., 2021). Additionally, the low activity of soil fauna resulting from the application of agrochemicals further adversely affected soil aggregation (Liao et al., 2015). Overall, these results emphasize the importance of land-use practices in influencing soil aggregation and highlight the potential benefits of vegetation restoration in enhancing soil health.

The preservation of aggregate stability is crucial for maintaining an optimal soil structure and preventing erosion, a critical aspect of sustainable land management (Zhu et al., 2022). In this study, cropland soil exhibited lower aggregate stability compared to other types of land use, as indicated by key indices such as WSA, MWD, GMD and St at the depth of 0–10 cm (Table 3). The study also highlighted a positive correlation between aggregate stability indices and OC contents within aggregates, suggesting that the increase in OC following land-use changes played a significant role in improving aggregate stability (Figs. 3–4). Furthermore, the high silt (e.g., in shrubland) and clay contents (e.g., in forestland) were also beneficial for enhancing soil aggregate stability (Fig. 3). Past studies in subtropical China have similarly documented the positive impact of land-use change involving afforestation on aggregate stability (Bai et al., 2020; Peng et al., 2023; Yu et al., 2023). Overall, transitioning cropland into grassland and forestland can potentially promote soil aggregate stability and diminish erosion risk more effectively than converting it into shrubland.

4.2. Land-use change impact on the distribution of OC and its fractions

The current study revealed that OC contents, in both bulk soil and

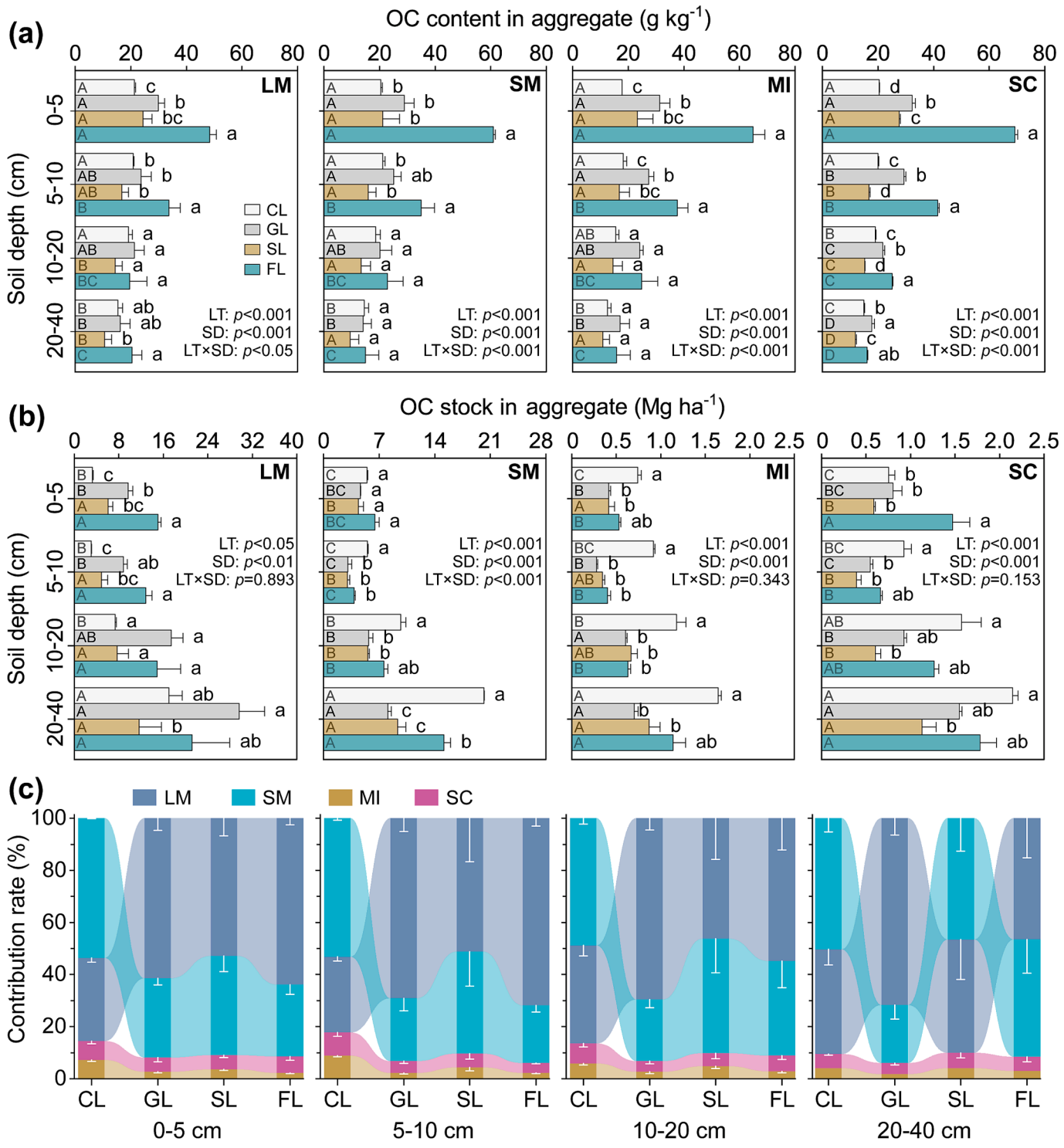

Fig. 4. Organic carbon (OC) content and stock (a–b) across different-sized aggregates and the contribution rate (c) of aggregates to soil OC under four land uses. Data are expressed as means and standard errors. Different lowercase letters within the same soil depth (SD) indicate significant differences ($p < 0.05$) among land-use types (LT). Different uppercase letters under the same LT indicate significant differences ($p < 0.05$) between SD. LT × SD indicates the interaction effect of both LT and SD. LM: large macroaggregate, SM: small macroaggregate, MI: microaggregate, SC: silt + clay. CL: cropland, GL: grassland, SL: shrubland, FL: forestland.

aggregates, showed a gradual decline as soil depth increased across all land uses (Figs. 2 and 4). This finding aligns with the result of Zhang et al. (2023), who also noted that the SOC showed an evident surface aggregation phenomenon in a tropical karst area. This should be related to distribution of organic matter in the soil profile. There was a noticeable reduction in aboveground litterfall input and belowground root biomass as soil depth increased, which would result in decreasing microbial activity and associated decomposition rate (Cheng et al., 2023; Peng et al., 2023). Consequently, the subsoil was characterized by lower SOC levels and its labile fraction compared to the topsoil (Pang et al., 2019; Wang et al., 2023). The average SOC content (24.55 g kg^{-1}) in the restored land uses was slightly lower than that (29.15 g kg^{-1} of karst regions in SW China and fell within the lower range of recorded values (2.67–117.74 g kg^{-1}) (Zhu et al., 2021), suggesting the karst soils

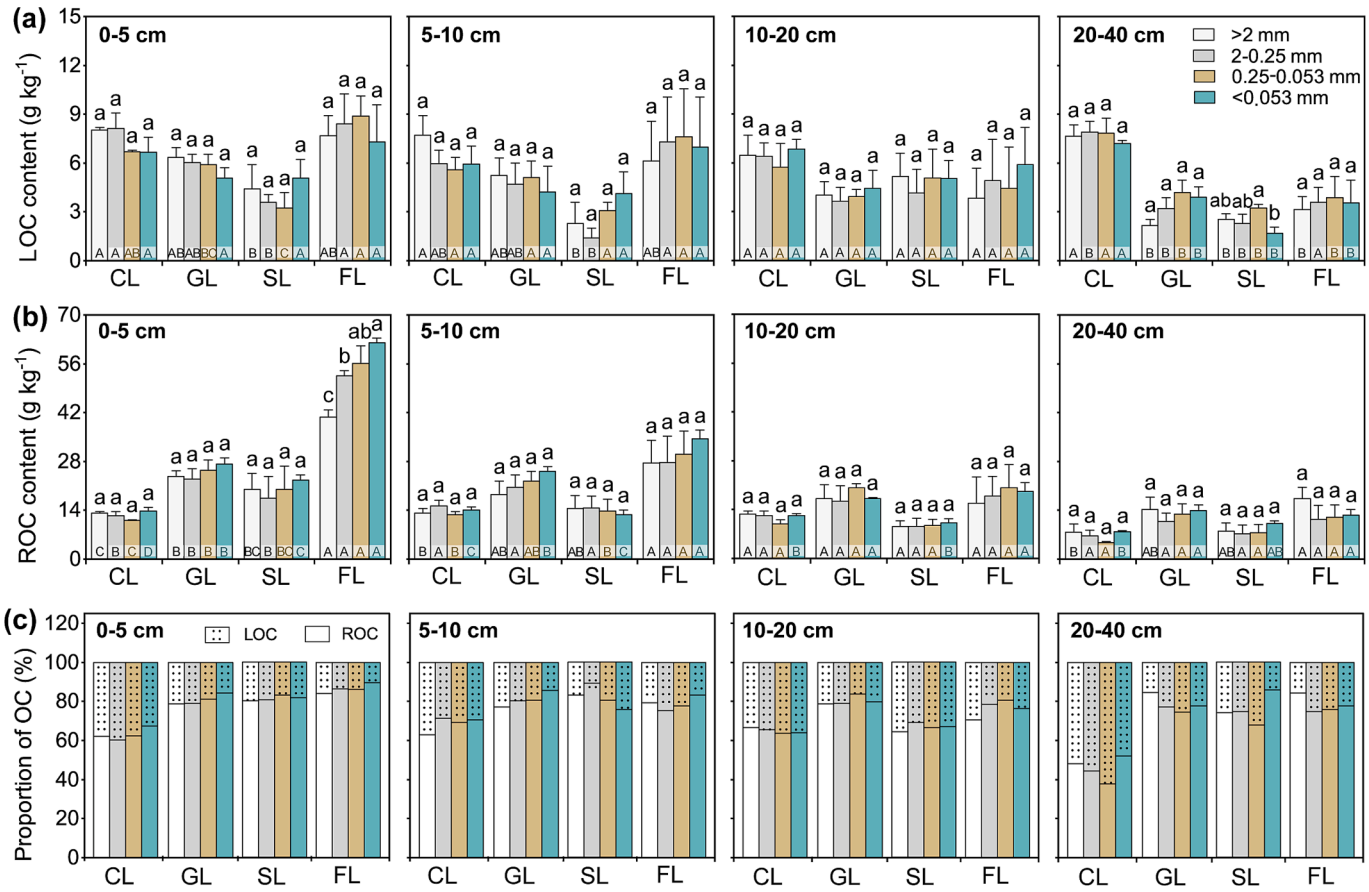

Fig. 5. The contents (a–b) and proportions (c) of labile and recalcitrant organic carbon (LOC and ROC) within different-sized aggregates under four land uses. Data are expressed as means and standard errors. Different lowercase letters under the same land-use type indicate significant differences ($p < 0.05$) among size classes. Different uppercase letters within the same size class indicate significant differences ($p < 0.05$) among land-use types. CL: cropland, GL: grassland, SL: shrubland, FL: forestland.

in the study area has great potential for C-sequestration.

Different land-use types and management practices play a critical role in shaping the SOC dynamics and its labile fractions (Liao et al., 2015; Yang et al., 2023). Long-term crop harvesting and tillage operations in agricultural lands not only reduce biomass return, but also weaken the physical protection of C through soil aggregates and accelerate soil C decomposition and loss (Liu et al., 2017; Bai et al., 2020). This was most likely the reason why lower levels of SOC (including ROC fraction) were observed under cropland than under grassland and forestland in the study (Fig. 2). Instead, vegetation restoration efforts directly contributed to an increase in organic matter input through plant litter and roots, and thus enhancing SOC accumulation (Peng et al., 2023). The LOC fraction exhibited a wide range of fluctuations across different land uses and accounted for 24.38–88.71 % of SOC (Fig. 2), which plays a significant role in predicting soil C pools (Blair et al., 1995). Interestingly, LOC contents and stocks remained the maximum values in the upper soil (0–5 cm) under forestland, while the maximum values were observed in the deeper soil layers (10–40 cm) under cropland (Fig. 2). This differential distribution of LOC levels may be attributed to the increased leaching erosion in cropland, leading to higher LOC levels in the deep soil (Zhang et al., 2023).

The storage and dynamics of OC and its fractions largely depends on the stability and particle size distribution of soil aggregates (Liao et al., 2015; Peng et al., 2023). In this study, we found a significant positive relationship between the mass proportion of macro-sized aggregate (LM and SM) and stocks of SOC and ROC ($p < 0.05$; Table 4), indicating that the macroaggregates were the primary contributors to SOC (a range of 82.16–93.92 %) across all land uses as revealed by the Fig. 4c. This result aligns with findings by Cheng et al. (2023) who reported that macroaggregates (> 0.25 mm) contributed the most to SOC, all reaching 90 % or more in the Loess Plateau, China. In the surface soil (0–5 cm), OC contents in macroaggregates were obviously lower than in microaggregates and silt + clay fractions (Fig. 4a), suggesting that small aggregates (< 0.25 mm) are important for the SOC storage under the restored land-use types. Under cropland, OC contents within aggregates were significantly positively correlated with LOC, while they were positively correlated with both LOC and ROC in other land uses ($p < 0.05$; Fig. 3; Table 4). This suggests that the variation in LOC under cropland has a more significant impact on SOC dynamics compared to the recalcitrant fraction. Additionally, the present results indicated that land use influenced the distribution of LOC within aggregates, with an increasing trend of LOC proportions with aggregate size at the 0–5 cm depth (Fig. 5). This was consistent with soil aggregate hierarchy theory (Six et al., 2000) and the results obtained by Burns et al. (2013) and Ma et al., (2022), who showed that labile C was predominantly found in macroaggregates and recalcitrant C was more concentrated in microaggregates or silt + clay fractions. However, the distribution of LOC proportions among size classes at the 5–40 cm depth varied across land-use types, demonstrating a heterogeneous distribution of aggregated-associated OC fractions throughout the soil profile.

4.3. Stable C isotope composition and aggregate-associated C flow pathways

Global land-use changes, particularly those related to variations in vegetation cover (C_3 *vs.* C_4 plants) with different ^{13}C signals, can

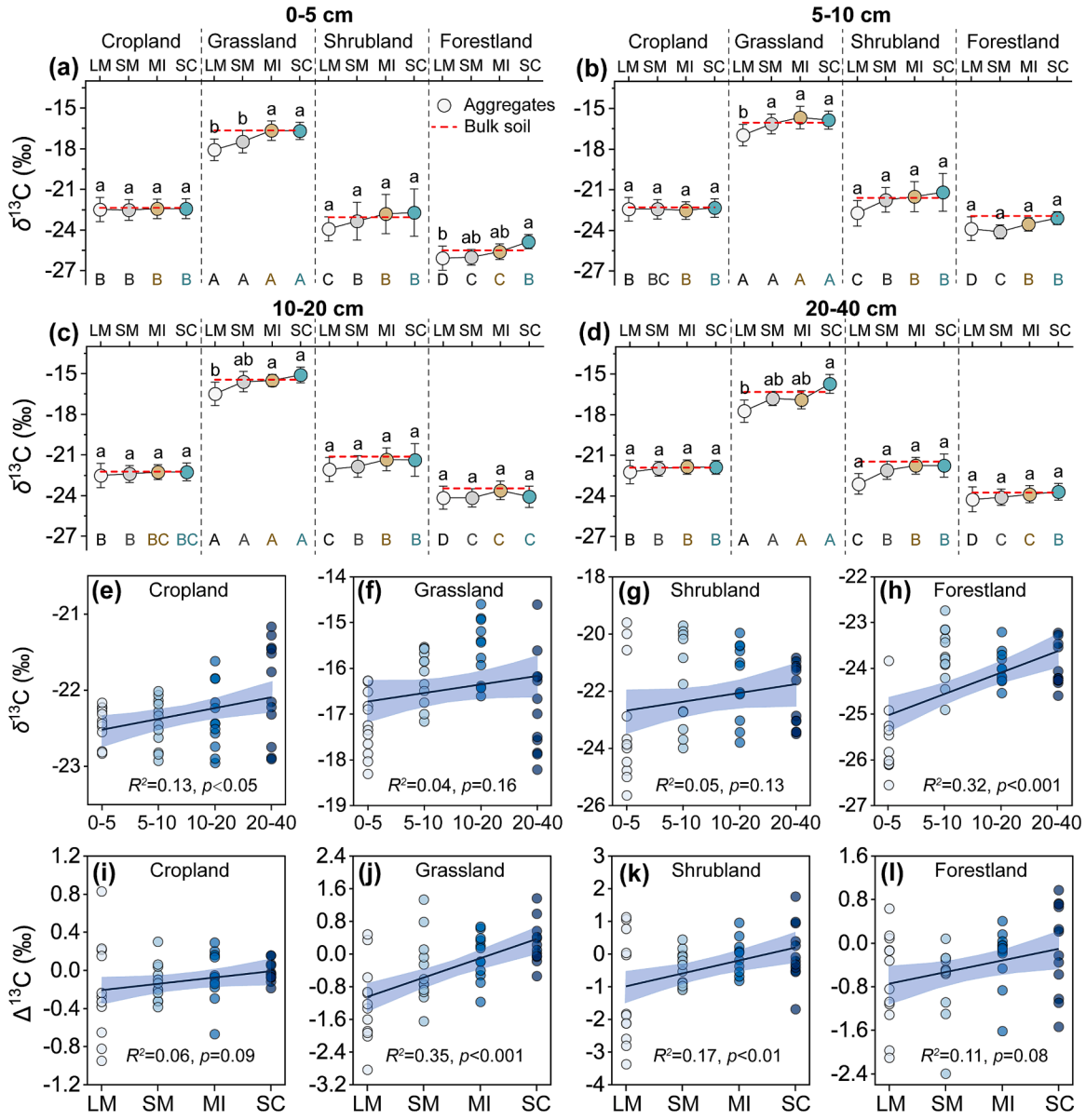

Fig. 6. Changes in $\delta^{13}C$ values (a–d) for bulk soil and different-sized aggregates under four land-use types. The images (e–l) show the variation patterns in the isotopic composition of soil aggregates with soil depth and aggregate size classes. The $\delta^{13}C$ values are expressed as means and standard errors. Different lowercase letters within the same land use indicate significant differences ($p < 0.05$) between different aggregate sizes. Different uppercase letters for the same aggregate size indicate significant differences ($p < 0.05$) among land-use types. The lines represent the variation patterns of $\delta^{13}C$ and $\Delta^{13}C$ values with soil depth and aggregate sizes, respectively. LM: large macroaggregate, SM: small macroaggregate, MI: microaggregate, SC: silt + clay.

influence the C isotope composition of SOC (Deng et al., 2016; Liu et al., 2018b; Zhao et al., 2024). This provided an opportunity to assess SOC dynamics in response to land-use transitions in that the $\delta^{13}C$ signature acts as a valuable tracer of C cycling and sequestration processes (Wang et al., 2022). In a certain ecosystem, higher $\delta^{13}C$ values are related to older OC, while lower $\delta^{13}C$ values are related to litterfall C input (Kohl et al., 2021; Shi et al., 2023). In the present study, the $\delta^{13}C$ values tended to decrease as vegetation restoration progressed. Any mechanism that promotes C turnover rate will accelerate the lighter ^{12}C loss, leading to a higher proportion of heavier ^{13}C. Therefore, the depletion of ^{13}C signified a slower cycling rate and less C loss, ultimately resulting in the enhancing soil stability as grasslands transition to forested areas. Specifically in grassland, bulk soil $\delta^{13}C$ values ranged from − 18.36 ‰ to − 14.53 ‰ (Fig. 6), indicating that SOC derived from C_4 vegetation. In other land uses, the wide range of $\delta^{13}C$ values (−26.23 ‰ to − 19.90 ‰) suggests that SOC originated from a mix of both C_3 and C_4 plants.

The $\delta^{13}C$ values generally increased as the aggregate sizes decreased along the land-use change (Fig. 6), which suggests that macroaggregates first formed and that old SOC was deposited in the silt + clay fractions. This was partially attributed to large aggregates contained younger OC that was less decomposed by microbes compared to smaller aggregates (< 0.25 mm) (Shi et al., 2023). However, the increasing trends in $\delta^{13}C$ from large particle sizes to small ones were not as prominent at depths of 0–20 cm under cropland due to frequent tillage disrupting aggregates and mixing soil layers. In general, the highest $\delta^{13}C$ values were identified within the silt + clay size classes, suggesting that OC in these classes had persisted longer or undergone more decomposition compared to OC in macro- and microaggregates (Six et al., 2000; Liu et al., 2018a). Furthermore, $\Delta^{13}C$ values tended to increase from large to small aggregates across all land-use types (Fig. 6). These results corroborated that: (a) isotopic fractionation during organic matter degradation led to an enrichment of ^{13}C in the residual SOC (Gunina and Kuzyakov, 2014;

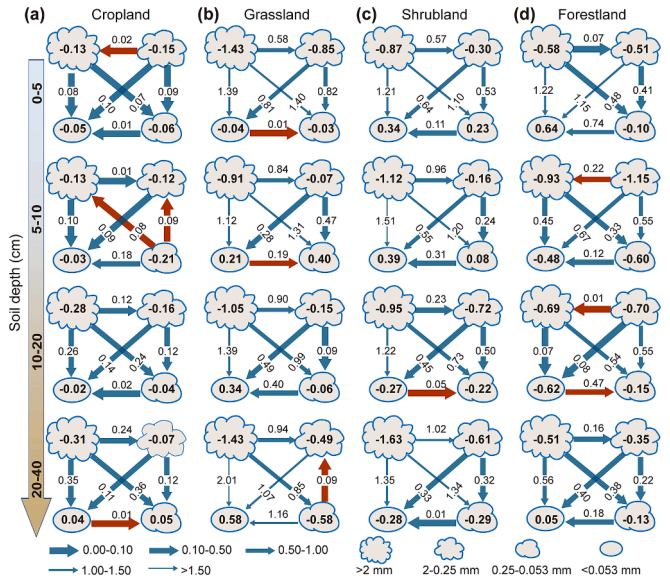

Fig. 7. Schematic diagram of the C flow pathways between soil aggregate size classes under different land uses. The numbers within cloud-shaped images represent the difference ($\Delta^{13}C$) between the $\delta^{13}C$ of the bulk soil and the $\delta^{13}C$ of the individual aggregate size class. Arrows indicate the direction of C flow from lower $\Delta^{13}C$ values to higher $\Delta^{13}C$ values, and the widths of the arrows reflect the probability of C flow between aggregate size classes. A wider arrow and a lower number (difference in $\Delta^{13}C$ value) above the arrows indicate a greater probability of C flow. The blue arrows (accounting for 89 %) indicate that the direction of C flow pathways from larger aggregates to smaller aggregates or silt + clay fraction, whereas the red arrows (accounting for 11 %) indicate the opposite direction of C flow.

Wang et al., 2022); and (b) plant-derived C was priority integrated into large aggregates that initially formed, while the old SOC was mainly preserved within the silt and clay particles.

The trends in C flows within the upper soil layer (0–5 cm) exhibited a decrease in intensity as vegetation restoration progressively (Fig. 7), reflecting the increased C loss and consequent ^{13}C enrichment under previously cultivated cropland and grassland. This shift indicates that the turnover of aggregates occurred at a faster rate in the early stages of vegetation restoration compared to later phase (e.g., shrub and forest), aligning with previous finding of Shi et al. (2023). Furthermore, it was found that C flows were stronger in the upper soil layers than in deeper soil (Fig. 7). On one hand, the rapid depletion of available LOC in the upper soil layer contributed to the increase in C flows (Figs. 2 and 7; Atere et al., 2020). Conversely, the slower C turnover rate in the deep soil was partly because of the accumulation of plant and microbial residues that have undergone prolonged decomposition, resulting in the formation of recalcitrant organic compounds enriched with ^{13}C (Fig. 6; Werth and Kuzyakov, 2008). Overall, the pathways of C flow within soil aggregates predominantly showed a pattern from macroaggregates to silt + clay fraction (Figs. 7 and 8), illustrating that C in macroaggregates functioned as a source while C in the silt + clay acted as a product.

4.4. Limitations of the present study

The present study highlighted the differences in aggregate-associated OC fractions and C sequestration mechanisms across various land-use types in a typical karst region. However, using natural ^{13}C abundance alone may not fully elucidate the complex impacts of changing vegetation and bedrock on C processes in karst soils (Han et al., 2020). To better understand how SOC is transformed, it is important to combine C and N isotopes or use isotope labeling techniques. By implementing these approaches, we can more accurately track the processes involved in C sequestration within karst environments.

5. Conclusions

Land-use conversion and soil depth significantly influenced soil aggregate distribution, aggregate-associated OC fractions, stocks, and C stabilization pathways in the Shilin karst area. Conventional cultivation practices had a detrimental effect on soil aggregation, resulting in a decrease in the mass proportions of macroaggregates and an increase in small aggregates in cropland compared to other land uses. However, vegetation restoration have shown promise in enhanceing aggregate stability and increasing the stocks of SOC, LOC, and ROC in the topsoil, It was observed that labile C tended to accumulate in macroaggregates, while recalcitrant C is more prevalent in small aggregates (< 0.25 mm). Macroaggregates were identified as the primary contributors to SOC across all land uses. The transition from grassland to forestland was associated with a decrease in the $\delta^{13}C$ of bulk soil, indicating reduced SOC decomposition and improved soil stability. The study also highlighted that C fluxes primarily occurred from macro- to micro-aggregates and silt + clay size classes, with cropland exhibiting higher

Table 4
Correlation coefficients between SOC content, stock in bulk soil and aggregate-associated mass proportion and OC content.

Aggregate size	SOC	LOC	ROC	SOC stock	LOC stock	ROC stock
Mass proportion						
LM	0.521***	0.227	0.641***	0.349*	0.116	0.436**
SM	−0.547***	−0.282	−0.638***	−0.317*	−0.109	−0.394**
MI	−0.353*	−0.031	−0.533***	−0.413**	−0.171	−0.497***
SC	−0.115	0.158	−0.307*	−0.260	−0.013	−0.369**
OC content						
LM	0.919***	0.808***	0.806***	0.079	0.109	0.049
SM	0.951***	0.795***	0.867***	0.081	0.068	0.076
MI	0.934***	0.738***	0.887***	0.091	0.038	0.109
SC	0.827***	0.626***	0.806***	−0.097	−0.135	−0.059
LOC content						
LM	0.122	0.214	0.022	−0.258	−0.149	−0.285*
SM	0.252	0.304*	0.155	−0.013	0.067	−0.059
MI	0.224	0.169	0.218	0.006	−0.004	0.011
SC	0.140	0.151	0.101	−0.096	−0.051	−0.109
ROC content						
LM	0.908***	0.769***	0.820***	0.152	0.153	0.129
SM	0.959***	0.780***	0.893***	0.089	0.057	0.095
MI	0.940***	0.744***	0.891***	0.094	0.040	0.113
SC	0.833***	0.622***	0.819***	−0.082	−0.131	−0.040

Note: * Significant at $p < 0.05$, ** Significant at $p < 0.01$, *** Significant at $p < 0.001$. LM: large macroaggregate, SM: small macroaggregate, MI: microaggregate, SC: silt and clay. SOC: soil organic carbon, LOC and ROC: labile and recalcitrant organic carbon.

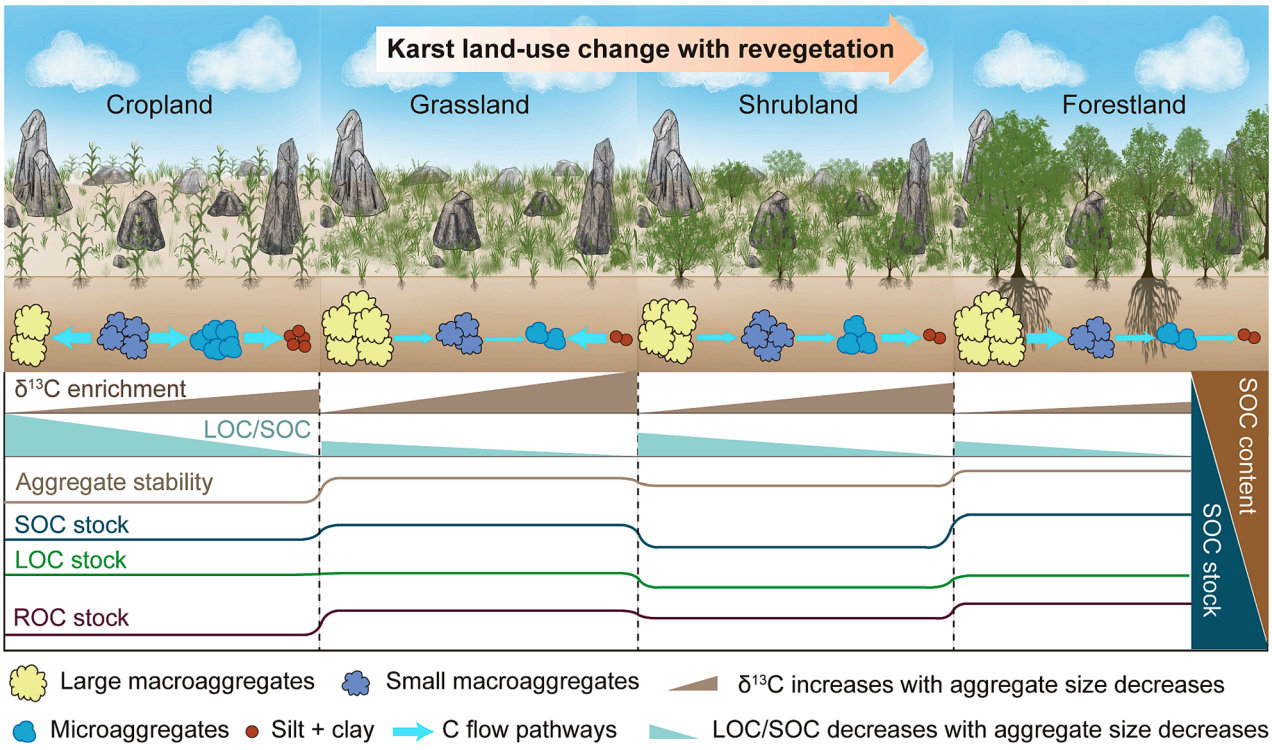

Fig. 8. Effect of land-use changes accompanying vegetation restoration on the soil aggregate stability, SOC dynamics, and C stabilization pathways in aggregates in a karst context. Note: Only the C stabilization pathways in the 0–5 cm soil depth are presented. The top of triangles indicate the average level of $\delta^{13}C$ or LOC/SOC values under different land uses. LOC: labile organic carbon, ROC: recalcitrant organic carbon.

intensity of C flows in the topsoil compared to other land uses. These findings provide valuable insights into the long-term SOC pool composition and C transformation processes in karst regions, emphasizing the roles of soil aggregate and its OC fractions under different land-use types. Appropriate land management and ecological restoration, such as grassland and forestland containing more SOC pools, maybe the preferred measures for long-term C sequestration in karst ecosystems of Southwest China.

CRediT authorship contribution statement

Xiai Zhu: Writing – original draft, Funding acquisition, Formal analysis, Conceptualization. **Youxin Shen:** Writing – review & editing, Visualization, Supervision. **Xia Yuan:** Investigation, Formal analysis, Data curation. **Ashutosh Kumar Singh:** Writing – review & editing, Formal analysis. **Liya Jin:** Investigation, Data curation. **Bin Yang:** Writing – review & editing, Supervision. **Chuang Yuan:** Investigation, Formal analysis. **Xiaojin Jiang:** Investigation, Formal analysis. **Wenjie Liu:** Supervision, Resources, Funding acquisition.

Declaration of competing interest

The authors declare that they have no known competing financial interests or personal relationships that could have appeared to influence the work reported in this paper.

Acknowledgements

The study was financially supported by the National Natural Science Foundation of China (32101380, 32371608 and 32271648), the 14th Five-Year Plan of the Xishuangbanna Tropical Botanical Garden, Chinese Academy of Sciences (E3ZKFF2B), and the Postgraduate Research and Innovation Foundation of Yunnan University (KC-23233905). We also acknowledged the assistance provided by the Xishuangbanna Station for Tropical Rainforest Ecosystem Studies and the Institutional Center for Shared Technologies and Facilities of Xishuangbanna Tropical Botanical Garden, CAS.

Data availability•

Karst soil carbon (Original data) ((Dryad))

References

An, J., Wu, Y.Z., Wu, X.Y., Wang, L.Z., Xiao, P.Q., 2021. Soil aggregate loss affected by raindrop impact and runoff under surface hydrologic conditions within contour ridge systems. Soil Tillage Res. 209, 104937.

Atere, C.T., Gunina, A., Zhu, Z.K., Xiao, M.L., Liu, S.L., Kuzyakov, Y., Chen, L., Deng, Y. W., Wu, J.S., Ge, T.D., 2020. Organic matter stabilization in aggregates and density fractions in paddy soil depending on long-term fertilization: Tracing of pathways by ^{13}C natural abundance. Soil Biol. Biochem. 149, 107931.

Bai, Y.X., Zhou, Y.C., He, H.Z., 2020. Effects of rehabilitation through afforestation on soil aggregate stanility and aggregate-associated carbon under forest fires in subtropical China. Geoderma 376, 114548.

Blair, G.J., Lefroy, R., Lisle, L., 1995. Soil carbon fractions based on their degree of oxidized, and the development of a carbon management index for agricultural systems. Aust. J. Agric. Res. 46 (7), 1459–1466.

Bossio, D.A., Cook-Patton, S.C., Ellis, P.W., Fargione, J., Sanderman, J., Smith, P., Wood, S., Zomer, R.J., Unger, M.V., Emmer, I.M., Griscom, B.W., 2020. The role of soil carbon in natural climate solutions. Nat. Sustain. 3, 391–398.

Burns, R.G., DeForest, J.L., Marxsen, J., Sinsabaugh, R.L., Stromberger, M.E., Wallenstein, M.D., Weintraub, M.N., Zoppini, A., 2013. Soil enzymes in a changing environment: current knowledge and future directions. Soil Biol. Biochem. 58, 216–234.

Cambardella, C.A., Elliott, E.T., 1993. Carbon and nitrogen distribution in aggregates from cultivated and native grassland soils. Soil Sci. Soc. Am. J. 57 (4), 1071–1076.

Cheng, Y.T., Xu, G.C., Wang, X.K., Li, P., Dang, X.H., Jiang, W.T., Ma, T.T., Wang, B., Gu, F.Y., Li, Z.B., 2023. Contribution of soil aggregate particle size to organic carbon and the effect of land use on its distribution in a typical small watershed on Loess Plateau. China. Ecol. Indic. 155, 110988.

Deng, L., Liu, G.B., Shangguan, Z.P., 2014. Land-use conversion and changing soil carbon stocks in China's 'Grain-for-Green' Program: a synthesis. Glob. Change Biol. 20 (11), 3544–3556.

Deng, L., Wang, K.B., Tang, Z.S., Shangguan, Z.P., 2016. Soil organic carbon dynamics following natural vegetation restoration: Evidence from stable carbon isotopes ($\delta^{13}C$). Agric. Ecosyst. Environ. 221, 235–244.
Dou, Y.X., Liao, J.J., An, S.S., 2023. Importance of soil labile organic carbon fractions in shaping microbial community after vegetation restoration. Catena 220, 106707.
Gasser, T., Crepin, L., Quilcaille, Y., Houghton, R.A., Ciais, P., Obersteiner, M., 2020. Historical CO_2 emissions from land use and land cover change and their uncertainty. Biogeosciences 17 (15), 4075–4101.
Guillaume, T., Damris, M., Kuzyakov, Y., 2015. Losses of soil carbon by converting tropical forest to plantations: erosion and decomposition estimated by $\delta^{13}C$. Glob. Change Biol. 21 (9), 3548–3560.
Gunina, A., Kuzyakov, Y., 2014. Pathways of litter C by formation of aggregates and SOM density fractions: Implications from ^{13}C natural abundance. Soil Biol. Biochem. 71, 95–104.
Guo, L.B., Gifford, R.M., 2002. Soil carbon stocks and land use change: A meta analysis. Glob. Change Biol. 8 (4), 345–360.
Han, G.L., Tang, Y., Liu, M., Zwieten, L.V., Yang, X.M., Yu, C.Y., Wang, H.L., Song, Z.L., 2020. Carbon-nitrogen isotope coupling of soil organic matter in a karst region under land use change. Southwest China. Agric. Ecosyst. Environ. 301, 107027.
Kohl, L., Myers-Pigg, A., Edwards, A., Billings, A., Warren, J., Podrebarac, A., Ziegler, E., 2021. Microbial inputs at the litter layer translate climate into altered organic matter properties. Global Change Biology 27, 435–453.
Li, J., Yuan, X., Ge, L., Li, Q., Li, Z., Wang, L., Liu, Y., 2020. Rhizosphere effects promote soil aggregate stability and associated organic carbon sequestration in rocky areas of desertification. Agric. Ecosyst. Environ. 304, 107126.
Liao, C., Chang, K.K., Wu, B.Y., Zhang, D.D., Wang, C., Cheng, X.L., 2024. Divergence in soil particulate and mineral-associated organic carbon reshapes carbon stabilization along an elevational gradient. Catena 235, 107682.
Liao, H.K., Long, J., Li, J., 2015. Soil organic carbon associated in size-fractions as affected by different land uses in karst region of Guizhou. Southwest China. Environ. Earth Sci. 74, 6877–6886.
Liu, M., Han, G.L., Zhang, Q., 2020. Effects of agricultural abandonment on soil aggregation, soil organic carbon storage and stabilization: Results from observation in a small karst catchment. Southwest China. Agric. Ecosyst. Environ. 288, 106719.
Liu, Y., Hu, C., Hu, W., Wang, L., Li, Z.G., Pan, J.F., Chen, F., 2018a. Stable isotope fractionation provides information on carbon dynamics in soil aggregates subjected to different long-term fertilization practices. Soil Tillage Res. 177, 54–60.
Liu, X., Li, L.H., Qi, Z.M., Han, J.G., Zhu, Y.L., 2017. Land-use impacts on profile distribution of labile and recalcitrant carbon in the Ili River Valley, northwest China. Sci. Total Environ. 586, 1038–1045.
Liu, Y., Liu, W.Z., Wu, L.H., Liu, C., Wang, L., Chen, F., Li, Z.G., 2018b. Soil aggregate-associated organic carbon dynamics subjected to different types of land use: Evidence from ^{13}C natural abundance. Ecol. Eng. 122, 295–302.
Ma, Y., Cheng, X.Q., Kang, F.F., Han, H.R., 2022. Effects of thinning on soil aggregation, organic carbon and labile carbon component distribution in Larix principis-rupprechtii plantations in North China. Ecol. Indic. 139, 108873.
Pang, D.B., Cui, M., Liu, Y.G., Wang, G.Z., Cao, J.H., Wang, X.R., Dan, X.Q., Zhou, J.X., 2019. Responses of soil labile organic carbon fractions and stocks to different vegetation restoration strategies in degraded karst ecosystems of southwest China. Ecol. Eng. 138, 391–402.
Pansu, M., Gautheyrou, J., 2007. Handbook of Soil Analysis: Mineralogical. Organic and Inorganic Methods. Springer Science & Business Media, Berlin, Heidelberg, New York, pp. 6–7.
Peng, X.Y., Huang, Y., Duan, X.W., Yang, H., Liu, J.X., 2023. Particulate and mineral-associated organic carbon fractions reveal the roles of soil aggregates under different land-use types in a karst faulted basin of China. Catena 220, 106721.
Qin, Z.C., Zhu, Y.K., Canadell, J.G., Chen, M., Li, T.T., Mishra, U., Yuan, W.P., 2024. Global spatially explicit carbon emissions from land-use change over the past six decades (1961–2020). One Earth 7 (5), 835–847.
Reynolds, W.D., Drury, C.F., Tan, C.S., Fox, C.A., Yang, X.M., 2009. Use of indicators and pore volume-function characteristics to quantify soil physical quality. Geoderma 152, 252–263.
Rong, G.H., Li, W.R., Zhu, H.S., Zhou, J.Y., Qiu, L.P., Ge, N.N., Wei, X.R., Shao, M.G., 2020. Dynamics of new-and old-organic carbon and nitrogen in bulk soils and aggregates following afforestation on farmland. Catena 195, 104838.
Shi, J.W., Deng, L., Gunina, A., Alharbi, S., Wang, K.B., Li, J.W., Liu, Y.L., Shangguan, Z. P., Kuzyakov, Y., 2023. Carbon stabilization pathways in soil aggregates during longterm forest succession: Implications from $\delta^{13}C$ signatures. Soil Biol. Biochem. 180, 108988.
Six, J., Paustian, K., Elliott, E.T., Combrink, C., 2000. Soil structure and organic matter: I. Distribution of aggregate-size classes and aggregate associated carbon. Soil Sci. Soc. Am. J. 64 (2), 681–689.
Tian, S.Q., Wang, S.J., Bai, X.Y., Luo, G.J., Li, Q., Yang, Y.J., Hu, Z.Y., Li, C.J., Deng, Y.H., 2021. Global patterns and changes of carbon emissions from land use during 1992–2015. Env. Sci. Ecotechnol. 7, 100108.
Wang, L.J., Luo, N.N., Shi, Q.L., Sheng, M.L., 2023. Responses of soil labile organic carbon fractions and enzyme activities to long-term vegetation restorations in the karst ecosystems. Southwest China. Ecol. Eng. 194, 107034.
Wang, K.L., Zhang, C.H., Chen, H.S., Yue, Y.M., Zhang, W., Zhang, M.Y., Qi, X.K., Fu, Z. Y., 2019. Karst landscapes of China: patterns, ecosystem processes and services. Landsc. Ecol. 34, 2743–2763.
Wang, X.Y., Zhao, L.X., Comeau, L.P., Bian, Q., Jiang, Y.J., Jiangdong, M., Chen, Y., Sun, B., 2022. Divergent carbon stabilization pathways in aggregates in Ultisols with and without organic amendments: Implications from ^{13}C natural abundance and NMR analysis. Geoderma 426, 116088.
Werth, M., Kuzyakov, Y., 2010. ^{13}C fractionation at the root-microorganisms-soil interface: A review and outlook for partitioning studies. Soil Biol. Biochem. 42 (9), 1372–1384.
Xiao, J.J., Zhao, Y.F., Wang, X., Hao, Z.G., Wang, K.C., Jiang, S.L., Liu, H.Y., Zhou, X.H., 2022. Effects of recovery models on organic carbon pathways: A method using $\delta^{13}C$ natural abundance. Agric. Ecosyst. Environ. 328, 107851.
Yang, F., Zhong, Y.J., Han, G.Z., Li, X.Z., Luo, L., Cai, X.M., Long, X.Y., Li, T.L., Huang, L. M., 2023. Effect of different vegetation restoration on soil organic carbon dynamics and fractions in the Rainy Zone of Western China. J. Environ. Manage. 331, 1107296.
Yu, P.J., Liu, J.L., Tang, H.Y., Ci, E., Tang, X.G., Liu, S.W., Ding, Z., Ma, M.G., 2023. The increased soil aggregate stability and aggregate-associated carbon by farmland use change in a karst region of Southwest China. Catena 231, 107284.
Zhang, B., Xu, C.H., Zhang, Z.H., Hu, C., He, Y.Y., Huang, K.K., Pang, Q.L., Hu, G., 2023. Response of soil organic carbon and its fractions to natural vegetation restoration in a tropical karst area, southwest China. Front. for. Glob. Change 6, 1172062.
Zhao, G.X., Cong, M.F., Zhang, Z.H., Zeng, F.J., Dong, X.P., Song, J.Y., 2024. Microaggregates regulate the soil organic carbon sequestration and carbon flow of windproof sand fixation forests in desert ecosystems. Catena 245, 108320.
Zhao, Z.M., Shen, Y.X., Wang, Q.H., Jiang, R.H., 2020. The temporal stability of soil moisture spatial pattern and its influencing factors in rocky environments. Catena 187, 104418.
Zheng, W., Rao, C.J., Wu, Q., Wang, E.W., Jiang, X.J., Xu, Y.C., Hu, L., Chen, Y.Z., Liang, X.C., Yan, W.D., 2022. Changes in the soil labile organic carbon fractions following bedrock exposure rate in a karst context. Forests 13 (4), 516.
Zhong, Z.K., Wu, S.J., Lu, X.Q., Ren, Z.X., Wu, Q.M., Xu, M.P., Ren, C.J., Yang, G.H., Han, X.H., 2021. Organic carbon, nitrogen accumulation, and soil aggregate dynamics as affected by vegetation restoration patterns in the Loess Plateau of China. Catena 196, 104867.
Zhu, X.A., Liu, W.J., Yuan, X., Chen, C.F., Zhu, K., Zhang, W.J., Yang, B., 2022. Aggregate stability and size distribution regulate rainsplash erosion: Evidence from a humid tropical soil under different land-use regimes. Geoderma 420, 115880.
Zhu, X.C., Ma, M.G., Tateno, R., He, X.H., Shi, W.Y., 2021. Effects of vegetation restoration on soil carbon dynamics in Karst and non-karst regions in Southwest China: a synthesis of multi-source data. Plant Soil 475, 45–59.